DAA Technical Memorandum OAR ETL-302

SENSITIVITY OF NUMERICAL SIMULATIONS OF MESOSCALE FEATURES ASSOCIATED WITH A LAND-FALLING CYCLONE TO MODEL PHYSICS

S.A. Michelson
J.-W. Bao

Environmental Technology Laboratory
Boulder, Colorado
February 2001

noaa NATIONAL OCEANIC AND ATMOSPHERIC ADMINISTRATION / Oceanic and Atmospheric Research Laboratories

NOAA Technical Memorandum OAR ETL-302

SENSITIVITY OF NUMERICAL SIMULATIONS OF MESOSCALE FEATURES ASSOCIATED WITH A LAND-FALLING CYCLONE TO MODEL PHYSICS

S.A. Michelson
CIRES, University of Colorado
Environmental Technology Laboratory

J.-W. Bao
Environmental Technology Laboratory

Environmental Technology Laboratory
Boulder, Colorado
February 2001

UNITED STATES DEPARTMENT OF COMMERCE

Donald L. Evans
Secretary

NATIONAL OCEANIC AND ATMOSPHERIC ADMINISTRATION

Scott B. Gudes
Acting Under Secretary for Oceans and Atmosphere/Administrator

Oceanic and Atmospl
Research Laboratorie

David L. Evans
Director

CONTENTS

ABSTRACT iii

1. INTRODUCTION 1

2. CASE DESCRIPTION 3

3. EXPERIMENT DESIGN 4
   a. Model configuration 4
   b. Sensitivity to physical parameterization schemes 4

4. SENSITIVITY TO PHYSICAL PARAMETERIZATON SCHEMES 6
   a. Cyclone movement and frontal structure 6
   b. Low-level wind in the warm sector 8
   c. The depth of the PBL across the cold front 10
   d. 12 hourly precipitation 12
   e. Cloud pattern 14
   f. .Bight region offshore and onshore winds 15
   g. Surface fluxes 16

5. DISCUSSION AND CONCLUSIONS 17

6. REFERENCES 19

7. FIGURE CAPTIONS 21

ABSTRACT

The focus of this study is to compare the mesoscale features of a land-falling cyclone simulated by a mesoscale model with various convective and planetary boundary layer (PBL) parameterization schemes. Significant sensitivity of the simulated mesoscale features to various parameterization schemes is revealed by comparison of the simulated frontal structure and the structure of a simulated low-level jet (LLJ). It is found that the quantity of onshore precipitation varies with different parameterization schemes, but the location of the maxima of precipitation does not. It is also found that while the PBL depth in the warm sector changes little with different parameterization schemes, in the cold sector behind the cold front it is sensitive to the choice of parameterization scheme. Moreover, different parameterization schemes appear to exert different impacts on the interaction between the LLJ and coastal topography, such as the blocking of low-level flow.

This study reveals that with certain permutations of the combination of the convective parameterization schemes and PBL schemes, the model produces an along-cold front variation of wind speed/vorticity. Observations are needed to validate this occurrence.

SENSITIVITY OF NUMERICAL SIMULATIONS OF MESOSCALE FEATURES ASSOCIATED WITH A LAND-FALLING CYCLONE TO MODEL PHYSICS

S.A. Michelson[1] J-W. Bao[2]

[1]CIRES, University of Colorado and NOAA/Environmental Technology Laboratory, Boulder, CO

[2]NOAA/Environmental Technology Laboratory, Boulder, CO

1. INTRODUCTION

Damaging wind and heavy rainfall events on the U.S. west coast are caused by land-falling oceanic extratropical cyclones that display a variety of mesoscale features. Because mesoscale features of the cyclones are of importance to coastal weather when interaction between the cyclones and coastal topography occurs, it is believed that an improvement in the predictability of the offshore mesoscale features such as tropospheric potential vorticity filaments/anomalies, frontogenesis and the low-level jet will lead to an improvement in the predictability of ensuing wind and precipitation onshore. Currently, prediction of the offshore mesoscale features relies mainly on numerical models because offshore upper-air observations are sparse. It is known that the development of extratropical cyclones results from the interaction of the so-called edge waves modulated by diabatic processes; the interaction is a function of the initial perturbations and the preconditioning of the large-scale environment, and the modulation is done by clouds/precipitation and surface fluxes. Inevitably, numerical model prediction of the mesoscale features of extratropical cyclones is affected by model initialization as well as model physics. Therefore, the evaluation of the sensitivity of the model prediction of the offshore mesoscale features of land-falling cyclones to model initialization and to choices of model physics is extremely useful for understanding the performance of numerical models in regional coastal wind and precipitation prediction.

To examine the sensitivity to initialization, special observations taken offshore are required along with different analyses from operational centers as the first-guess fields. Over the

past few years, field experiments have been carried out to test the hypothesis that observations taken in a limited area offshore, if targeted well for local coastal prediction, can improve the predictability of the near-shore mesoscale features of land-falling cyclones. Preliminary results from past experimental data impact studies using these offshore targeted observations indicate that observations of some offshore mesoscale features associated with land-falling cyclones, by intrinsic dynamics, have more positive impact on coastal wind and precipitation prediction than observations of other mesoscale features. For example, the observations of the mid- and lower-tropospheric temperature and wind perturbations around the westerly upper-level jet have more impact on the ensuing coastal wind and precipitation than the observations of temperature and wind within the low-level jet (see, e.g., Langland et al., 1999, and Bao et al., 2000).

Many case studies and idealized numerical simulations show that mesoscale features of extratropical cyclones are not only sensitive to the initial perturbations and the large-scale environmental setting, but also to the physical processes of moist convection and surface fluxes of momentum, latent heat, and sensible heat. Although realistic cyclogenesis can be produced in numerical models by purely adiabatic processes, physical processes lead to different evolutions of the mesoscale features of the cyclone system. For example, over the ocean, saturation behind the cold front occurs due to surface heat and moisture fluxes and planetary boundary layer mixing, producing stratocumulus clouds in the cold air behind the cold front. This is often accompanied by a deep cloud band and transverse circulation over the surface cold front. As a result, the horizontal temperature gradient in the cold air becomes relatively weak because the latent heating in the stratocumulus clouds and the upward sensible heat flux counteract the cold advection behind the front. Different physical parameterization schemes for surface fluxes and moist convection, due to synergism of their interaction, can certainly produce different effects on the mesoscale processes associated with the cold front. These different effects can also be complicated by interaction of the cold front with the coastal topography.

The focus of this report is to compare the mesoscale features of a land-falling cyclone simulated by a mesoscale model with various convective and planetary boundary layer parameterization (PBL) schemes. It is intended to reveal the model's sensitivity to different parameterization schemes for the purpose of understanding the performance of the model in wind and precipitation predictions over the U.S. west coast. The report is organized as follows. A

brief description of the case used in the study will be provided in section 2. Aspects of numerical experiments will be described in section 3. Then, the sensitivity to model parameterizations will be explored in section 4, which is followed by discussion and summary in section 5.

2. CASE DESCRIPTION

The case chosen for this study is the cyclone system that made landfall along the California coast on 2-3 Feb 1998. Figure 1 shows satellite images that reveal the evolution of the large-scale pattern associated with the cyclone system. Surface analyses (Fig. 2) based on ship and buoy reports, as well as NOAA P-3 in situ flight level data, indicate that there were actually two frontal systems offshore at 1200 UTC Feb 2: a low center with the leading cold front and a warm front extending from this low eastward and into the bight region of southern California, and a second cold front associated with a developing low center (Fig. 2a). As these frontal systems progressed eastward, the first low center decayed. By 0000 UTC Feb 3, the trailing cold front began to catch up with the leading cold front, and the developing low center took over as the main low center of the entire system (Fig. 2b). This double structured frontal system is persistent as the system made landfall at 1200 UTC Feb 3 (Fig. 2c) and is also apparent in radar and profiler data (not shown).

The land-falling event involved two stages. The first was associated with a northward advance of a warm front, which produced up to 177 mm (7.0 inches) of rain in the coastal mountains in the 24 hours ending at 1800 UTC 2 February. The second stage was associated with the landfall of the LLJ and cold front southeast of the cyclone center on 3 Feb. In the second stage, the pre-frontal LLJ brought significant winds and flooding to the coastal regions of California. The interaction of the LLJ with the terrain was regarded as a major factor in the severe weather that occurred during this weather event, including the 314 mm (12.4 inches) of rain that fell in the 24 h period from 1800 UTC 2 Feb to 1800 UTC 3 Feb in the coastal mountains near Monterey. Most of the discussion of the numerical sensitivity experiments will be focused on the second stage, while the sensitivity of the simulated warm front to model physics will be briefly mentioned.

3. EXPERIMENT DESIGN

3a. Model configuration

The numerical model used in this study is the nonhydrostatic version of the Pennsylvania State University/National Center for Atmospheric Research (NCAR) mesoscale modeling system (MM5) (Grell et al., 1994). The set of grids used is doubly nested: a 36-km-resolution grid (121 by 121 grid points) covering most of the western United States and a large portion of the eastern Pacific Ocean; and a 12 km grid (166 by 166 grid points) covering California, Oregon, and the Pacific Ocean out to about 140°W (Fig. 3). A total of 50 σ layers are used, with the lowest layer at about 15 m above ground level. In all the experiments, the interaction between the 36 km and 12 km grids is two-way.

The model is initialized at 0000 UTC 2 Feb 1998 and all simulations are carried out for 48 hours. The gridded data used to initialize the model are obtained by performing a successive-scan objective analysis on conventional surface and rawinsonde observations. The first-guess fields are the gridded global analyses of wind, temperature, geopotential, and relative humidity at the mandatory levels from the National Centers for Environmental Prediction (NCEP). However, the sea-surface temperature data for the initial conditions are obtained from the sea-surface temperature (SST) analysis of the advanced very high resolution radiometer (AVHRR) data set which is interpolated to the MM5 36-km coarse mesh.

3b. Sensitivity to physical parameterization schemes experiment design

In order to determine the sensitivity to model PBL and convective parameterization schemes, 12 simulations are carried out with different combinations of model physics. Table 1 illustrates all the possible combinations of PBL and convective parameterization schemes that are tested in this study. There are four PBL schemes tested: MRF (Hong and Pan, 1996), Blackadar (Blackadar, 1979), Burk-Thompson (Burk and Thompson, 1989), and ETA (Janjić, 1994) schemes. There are three convective parameterization schemes tested: Kain-Fritsch (Kain and Fritsch, 1993), the Anthes-Kuo scheme (Anthes, 1977) scheme, and the Grell scheme (Grell,

1993). The same physical parameterization schemes are applied to both the 36- and 12- km grids in all experiments. On both grids and in all of the experiments the simple ice explicit moisture scheme (Dudhia, 1993) is used.

Table 1. Model configurations for the physical parameterization sensitivity experiments

Experiment Name	PBL Scheme	Convective Scheme
MRFKF	MRF	Kain-Fritsch
MRFAK	MRF	Anthes-Kuo
MRFGRELL	MRF	Grell
BLACKKF	Blackadar	Kain-Fritsch
BLACKAK	Blackadar	Anthes-Kuo
BLACKGRELL	Blackadar	Grell
ETAKF	ETA	Kain-Fritsch
ETAAK	ETA	Anthes Kuo
ETAGRELL	ETA	Grell
BTKF	Burk-Thompson	Kain-Fritsch
BTAK	Burk-Thompson	Anthes-Kuo
BTGRELL	Burk-Thompson	Grell

It should be point out that among all the convective parameterization schemes, the Anthes-Kuo scheme is the one whose physical merits have been criticized (see, e.g., Raymond and Emanuel, 1993). The reason that is was used in this study is that, despite the criticism, the scheme is still used as an option in a few popular 3-D primitive equations models. Some mesoscale forecasting studies (see, e.g., Wang and Seaman, 1997) indicate that it can perform comparably to the other aforementioned schemes. In our previous study (Bao et al,. 2000) on the impact of the California Land Falling Jets Experiment (CALJET) data on numerical coastal wind and precipitation prediction, it was found that the Anthes-Kuo scheme, among other schemes available in MM5, produced the cyclone movement that was closest to observational analysis. Moreover, the Anthes-Kuo scheme is still used in numerical regional/global climate sensitivity

studies (Somerville, 2000). More evaluation of the performance of the Anthes-Kuo scheme is needed to further understand its performance in forecasting short time scales and climate studies.

4. SENSITIVITY TO PHYSICAL PARAMETERIZATION SCHEMES

4a. Cyclone movement and frontal structure

All the experiments successfully reproduce the development of the second low center depicted in Figure 3. The cold front associated with this low center later catches up with the leading cold front, and the low center itself evolves into a cyclone with doubly structured cold fronts. Since the movement of the simulated system is controlled by its interaction with the large-scale setting defined in the initial and boundary conditions, there is little difference in the moving direction of the simulated cyclone. However, the details of the simulated cyclone and its mesoscale features show noticeable differences because they are influenced by the physical parameterizations.

As for the development of the cyclone center, the results of all the sensitivity experiments can be categorized into two scenarios, which are shown in Figure 4 for 1200 UTC 3 Feb. One scenario has a cyclone with two separate low centers, (Fig. 4a), while the other has only one (Fig. 4b). No matter which PBL scheme is used with the Anthes-Kuo convective scheme and no matter which convective scheme is used with MRF PBL scheme, only one low center is produced. When the Kain-Fritsch convective scheme is used, two centers are produced with every PBL scheme except for the MRF scheme. The Grell convective scheme, when used with the MRF and ETA PBL schemes, produces two centers. However, when used with the Burk-Thompson or MRF PBL scheme, it produces one center. This suggests that the interaction between the convective and PBL schemes is complicated, and make it difficult to pinpoint whether the PBL scheme or convective scheme has more effect in producing the two centers. It should be noted that the overall orientation of the trough is quite similar in all of the experiments. This is especially true at 1200 UTC 3 Feb (Fig. 4). While some of the experiments produce two low centers, and others produce only one, there is always a north-south elongated trough.

Moreover, the orientation of the simulated cold fronts in all the experiments appear similar to each other.

While the cold fronts in all of the experiments look fairly similar, the warm fronts do exhibit some sensitivity to the physical parameterizations. Overall, the warm fronts are more sensitive to the convective schemes than to the PBL schemes. Furthermore, the differences are greatest when the experiments with the Anthes-Kuo convective scheme are compared with either the experiments with the Kain-Fritsch or those with the Grell convective scheme. In the experiments with the Anthes-Kuo scheme, the warm front has a more north/south orientation than the warm front in the experiments with the other two convective schemes (not shown).

In all of the experiments, except for those using the Anthes-Kuo convective scheme, the cold front exhibits a double structure offshore. This double structure can most clearly be seen in the low-level equivalent potential temperature field (Fig. 5). The greatest difference is again seen when the experiments with the Anthes-Kuo convective scheme are compared to the experiments using the other convective schemes. The cellular pattern of the equivalent potential temperature seen in Figure 5b when using the Anthes-Kuo scheme is similar no matter which PBL scheme is used. There are noticeable differences between the experiments with the Grell and the Kain-Fritsch convective schemes. For example, in Figure 5a and Figure 5c, the double structure of the cold front is more apparent when the Kain-Fritsch scheme is used.

The double structure is also apparent when a cross section is taken across the cold fronts. Figure 6 shows cross sections of the equivalent potential temperature at the same time (1500 UTC 2 Feb) as the horizontal plots of equivalent potential temperature in Figure 5; the locations of the cross sections are shown by the lines AB and CD in Figure 5a and Figure 5c. The experiment with the Anthes-Kuo scheme is not shown because it does not show a distinct double structure. These cross sections clearly show the sensitivity of the cold frontal system to the convective schemes. There is a pocket of colder and drier air in between the two cold fronts when the Grell scheme is used. Additionally, in the experiment with the Grell scheme, the air is colder behind cf1 than in the experiment with the Kain-Fritsch scheme. It is interesting to note that the pocket of colder and drier air between cf1 and cf2 comes from aloft. This structure appears to resemble the one that serves as an important role in making the cold front split in the conceptual model of split cold front that was first shown by Browning and Monk (1982) and later summarized by

Bader et al. (1995, section 4.2). However, because there is a remnant of a previously developed cold front (cf1) ahead of the newly developing one (cf2), the ensuing development of the double frontal structure becomes different from the above conceptual model (not shown).

4b. Low-level wind in the warm sector

One of the important mesoscale features of land-falling cyclones on the U.S. west coast is the LLJ. Because the LLJ is part of the cyclone system, its evolution can be affected by the choice of model physics. To examine the LLJ's sensitivity to model physics, all the experiments are first compared in terms of the height of the maximum wind speed within the offshore pre-frontal LLJ. In this comparison, the height of the LLJ is taken at approximately the same location along the front and is the height of the maximum low-level wind. Figure 7 shows the offshore height of the LLJ at 1800 UTC 2 Feb as a function of convective schemes. This figure indicates that the MRF PBL scheme consistently produces a higher LLJ than the other PBL schemes no matter which convective scheme is chosen. It is also shown in Figure 7 that for each PBL scheme, the Kain-Fritsch convective scheme produces a higher LLJ than the other convective schemes. Additionally, there is a pattern of the highest to lowest height of the LLJ with all three convective schemes. The MRF PBL scheme has the highest, as previously mentioned, followed by the Blackadar, ETA, and finally Burk-Thompson scheme.

The comparison of the maximum wind speed within the LLJ core is also carried out. There does not seem to be a coherent pattern of the sensitivity of the maximum wind speeds as a function of convective schemes (Fig. 8). Although for both the Kain-Fritsch and Anthes-Kou schemes, the maximum wind speed at the core of the LLJ increases with the sequence of the MRF, Blackadar, and ETA schemes, for the Grell scheme the Blackadar scheme produces the highest wind speed. The MRF PBL scheme has a lower maximum wind speed for all convective schemes than the Blackadar, ETA, or Burk-Thompson scheme at 1800 UTC (Fig. 8). There is no clear pattern when the PBL scheme is varied. The Grell scheme produces the fastest LLJ with all PBL schemes except the ETA at 1800 UTC, while the Anthes-Kuo scheme produces the slowest LLJ with all PBL schemes except for the ETA PBL scheme (although the maximum speed of 38 m/s is the same as when the ETA PBL scheme is run with the Grell convective scheme).

Clearly, varying both the convective and the PBL schemes can have an impact on the height of the LLJ and the maximum wind speed of the LLJ. Changing the convective scheme can vary the height of the LLJ as much as 540 m (as seen in Table 2), while changing the PBL scheme can vary the height of the LLJ by as much as 680 m (Table 3). Changing the convective scheme can vary the maximum speed of the LLJ by as little as 0.94 m/s to as much as 2.94 m/s (Table 4), while changing the PBL scheme can vary the maximum speed by as little as 1.41 m/s and as much as 2.87 m/s (Table 5).

Table 2. Standard deviation of the height of the LLJ (m) for each PBL scheme when varying the convective scheme.

PBL scheme	Standard Deviation (m)
MRF	540.
Blackadar	240.
ETA	140.
Burk-Thompson	50.

Table 3. Standard deviation of the height of the LLJ (m) for each convective scheme when varying the PBL scheme.

Convective scheme	Standard Deviation (m)
Kain-Fritsch	680.
Anthes-Kuo	230.
Grell	550.

Table 4. Standard deviation of the maximum speed of the LLJ (m/s) for each PBL scheme when varying the convective scheme.

PBL scheme	Standard Deviation (m/s)
MRF	2.05
Blackadar	2.45
ETA	0.94
Burk-Thompson	2.94

Table 5. Standard deviation of the maximum speed of the LLJ (m/s) for each convective scheme when varying the PBL scheme.

Convective scheme	Standard Deviation (m/s)
Kain-Fritsch	1.41
Anthes-Kuo	2.69
Grell	2.87

In addition to the sensitivity of the height and intensity of the LLJ, the horizontal wind speed distribution in the warm sector ahead of the cold front appears to vary with different convective and PBL schemes. For example, in the experiment using the Burk-Thomspson PBL and Kain-Fritsch convective schemes, the offshore distribution of the wind ahead of the cold front 18 hours later, when the cold front gets closer to the coast, the gradient of wind speed becomes fragmented with multiple maxima (Fig. 9b). However, for the experiment using the MRF PBL and the Grell convective scheme, there is a near uniform gradient of wind speed along the cold front at 1200 UTC 2 Feb (Fig. 10a). The near uniform gradient of wind speed ahead of the cold front does not change before the cold front makes landfall (Fig. 10b). No observations for this case are available to validate the along-front variation of wind distribution in the experiment using the Burk-Thomspson PBL and Kain-Fritsch convective schemes. To the authors' best knowledge, not much evidence is available in the literature to strongly prove or disprove the possibility of the gradient of wind speed becoming fragmented. However, the analyses carried out by Hobbs and Persson (1982) suggest that it could occur in reality.

4c. The depth of PBL across the cold front

The sensitivity of the PBL height to varying physical parameterization schemes is investigated by comparing the depth of the PBL behind the cold front (where the PBL becomes more homogeneous) while it is still offshore at 1800 UTC 2 Feb (Table 6). It is clear that the convective parameterization scheme can play an important role in determining the PBL height. For example, for both the Blackadar and ETA PBL schemes, the PBL heights differ by 500 m between convective schemes, with the Anthes-Kuo scheme producing the highest PBL height for

both PBL schemes. However, with the MRF PBL scheme, there is no difference in the PBL height. It appears the convective scheme can play an important role in determining the PBL depth. By changing the convective scheme, the depth of the PBL can vary as much as 410 m, while varying the PBL scheme the depth of the PBL varies only as much as 259 (see Tables 7 and 8).

Table 6. Depth of the PBL for each experiment offshore at 1800 UTC 2 Feb.

Experiment	PBL Height (km)
MRFKF	1.6
MRFAK	1.6
MRFGRELL	1.6
BLACKKF	1.0
BLACKAK	2.0
BLACKGRELL	1.5
ETAKF	1.0
ETAAK	2.0
ETAGRELL	1.5
BTKF	1.0
BTAK	1.5
BTGRELL	1.4

Table 7. The standard deviation of the depth of the PBL (m) for each PBL scheme when varying the convective scheme.

PBL scheme	Standard Deviation (m)
MRF	0.0
Blackadar	410.
ETA	410.
Burk-Thompson	374.

Table 8. The standard deviation of the depth of the PBL (m) for each convective scheme when varying the PBL scheme.

Convective scheme	Standard Deviation (m)
Kain-Fritsch	259.
Anthes-Kuo	227.
Grell	70.

By and large, the depth of the PBL in the warm sector exhibits far less sensitivity to the physical parameterizations than the depth of the PBL in cold air behind the cold front. Additionally, the depth of the PBL in the warm sector (~1 km) is shallower than the depth in the cold air.

4d. 12 hourly precipitation

To look at the sensitivity of the onshore precipitation to the physical parameterizations, the 12-h accumulated precipitation ending 1200 UTC 3 Feb is compared. This time period encompasses the northward advancement of the warm front along the central and northern California coast and the landfall of the LLJ to the south, thus capturing a significant amount of the heavy precipitation for this event.

In all of the experiments, there are four maxima in common: one area in the bight region of southern California near Santa Barbara, one along the Sierra Nevada Mountains in central California, one along the coast south of Monterey, and one in northern California. The spatial precipitation patterns for all the experiments with the Grell and Kain-Fritsch convective schemes are fairly similar. However, the experiments using the Anthes-Kuo scheme have a gap in the precipitation in central California that is not present when the other two convective schemes are used (Fig. 11).

A detailed comparison of the rainfall in the bight region of California reveals the sensitivity of the onshore precipitation to the physical parameterizations. The precipitation in this area is orographically enhanced as the LLJ and southerly flow ahead of the cold front impinges on the higher terrain to the north of Santa Barbara. Table 9 shows the maximum precipitation amounts for the 12 h interval ending at 1200 UTC 3 Feb for all the experiments in the Santa

Barbara area. From this table, it is evident that experiments with the Anthes-Kuo convective parameterization scheme produce significantly higher precipitation amounts, on the order of 2-3.0 times more precipitation than the experiments with the Grell and Kain-Fritsch convective schemes (203-230 mm in 12 h compared to 74-95 mm in 12 h for Grell and Kain-Fritsch experiments). While the maximum amount of precipitation varies, the different locations of the maxima appear to relate more to the low-level wind direction relative to the ridges of topography than to the physics.

At first glance, the precipitation maxima list in Table 9 indicate that there are far fewer differences in the precipitation maxima when the PBL scheme is changed. For example, with the Anthes-Kuo convective parameterization scheme, the least difference when varying the PBL schemes is as small as 7 mm in 12 h while at most the difference is as much as 16 mm in 12 h (using the Kain-Fritsch scheme). This difference is far less than the difference when varying the convective scheme. This seems to suggest that the variation in the precipitation maxima is

Table 9. Maximum 12-h accumulated precipitation ending at 1200 UTC 3 Feb near Santa Barbara, CA for all 12 experiments.

Experiment	12-h accumulated precipitation near Santa Barbara, CA (mm)
MRFKF	88
MRFAK	230
MRFGRELL	92
BLACKKF	80
BLACKAK	222
BLACKGRELL	74
ETAKF	77
ETAAK	223
ETAGRELL	92
BTKF	93
BTAK	203
BTGRELL	95

likely to be caused more by the differences in the convective schemes than by the differences in the PBL schemes. However, careful examination of Table 9 shows that the dominance of the sensitivity to the convective schemes is exaggerated by the much larger precipitation maxima from the experiments using the Anthes-Kuo scheme. When excluding all the experiments using the Anthes-Kuo scheme, the variation in the precipitation maxima is more sensitive to the PBL schemes than to the convective schemes. The standard deviations shown in Table 10 and Table 11 clearly indicate this.

Table 10. Standard deviation of precipitation (mm) for each PBL scheme when varying the convective scheme with and without the experiments with the Anthes-Kuo scheme included.

PBL scheme	Standard Deviation with Anthes-Kuo scheme included (mm)	Standard Deviation (mm) without Anthes-Kuo scheme included
MRF	66.0	2.0
Blackadar	68.4	3.0
ETA	65.6	7.5
Burk-Thompson	51.4	1.0

Table 11. Standard deviation of precipitation (mm) for each convective scheme when varying the PBL scheme.

Convective scheme	Standard Deviation (mm)
Kain-Fritsch	6.3
Anthes-Kuo	10.0
Grell	8.3

4e. Cloud pattern

The model simulated dBz shows an interesting sensitivity to the convective scheme and may shed some light as to why the Anthes-Kuo scheme produces significantly more precipitation. The model simulated dBz (Fig. 12) in both the Grell and Kain-Fritsch schemes are similar,

indicating a fairly wide and continuous swath of clouds associated with the frontal system. However, the simulated dBz in the Anthes-Kuo experiments appear to be less organized and more cellular in pattern. Moreover, there are fewer clouds associated with the fronts in the Anthes-Kuo experiments. All of these patterns are not only seen in the dBz, but also are seen in the cloud water field as well as rain water field (not shown). Since, as noted before, the Anthes-Kuo experiments produce more precipitation than the experiments with other schemes in the bight region, the difference in the cloud pattern indicates that with the Anthes-Kuo convective scheme, more water vapor is converted into precipitation rather than to cloud water and/or rain water as compared to either the Grell or Kain-Fritsch schemes.

Despite the similarities among the experiments using the Grell and Kain-Fritsch convective schemes, mesoscale differences do occur. For instance, the dBz pattern in coastal northern California is different. The band of higher dBz values just inland in northern California is stronger when the Kain-Fritsch scheme is used. Also, the dBz values associated with the cold front in southern California seem to indicate a more banded cold frontal structure when the Grell scheme is used (compare Fig. 12a to Fig. 12c).

4f. Bight region offshore and onshore winds

There are differences in the flow in the warm sector as the cold front and pre-frontal LLJ approach the bight region in southern California with varying physical parameterizations. Two wind profiles are extracted from the model output for each experiment: one from a point offshore in the bight region of California, just west of San Clemente Island and Santa Catalina Island and the other point onshore near Santa Barbara, CA. Figures 13 and 14 show time-height series for the offshore (Fig. 13) and onshore (Fig. 14) points from 1800 UTC 2 Feb to 1200 UTC 3 Feb for the Blackadar PBL scheme with varying convective schemes. Offshore, it is clear that the fast low-level flow (> 25 m/s) ahead of the cold front starts to appear earlier and extends lower when the Anthes-Kuo scheme (Fig. 13b) is used than when either the Kain-Fritsch (Fig. 13a) or the Grell (Fig. 13c) convective scheme is used. This could be one reason why the experiments using the Anthes-Kuo scheme produce more precipitation; that is, the experiments with the Anthes-Kuo

scheme produce low-level convergence on the windward side of the mountains in the region that lasts longer to produce more subgrid convection than those from other experiments. The flow at the onshore point also indicates a sensitivity; in particular, the blocking of flow by the mountains lasts longer when the Anthes-Kuo convective scheme is used (e.g., see Fig. 14) compared to when the other convective schemes are used.

Despite the sensitivity of the onshore and offshore winds to physics parameterization schemes, the timing of the cold front landfall shows little difference in all the simulations (not shown). This suggests that the difference in all the parameterization schemes is not a crucial factor to the frontal propagation.

4g. Surface fluxes

A comparison of all the experiments in the bight region indicates the sensitivity of the surface latent and sensible heat fluxes to the physics parameterization schemes. To illustrate this, the sensible and latent heat fluxes at 0900 UTC 3 Feb are compared (Fig. 15). The time of 0900 UTC is chosen because a significant amount of the precipitation shown in Figure 11 occurs between 0600 UTC and 1200 UTC 3 Feb. The sensible and latent fluxes for the experiments with the Anthes-Kuo convective scheme also are significantly higher than with the other convective schemes. For example, within the experiments with the Blackadar PBL scheme, when the Anthes-Kuo scheme is used, the sensible heat flux is about 3-4 times as much off the coast near Point Conception region as it is with either the Kain-Fritsch or Grell convective schemes. The latent heat fluxes in this area also display a difference (~ 3-4 times, not shown). There are also differences in the pattern for both the latent and sensible heat fluxes. For example, because the air is colder and drier and the wind is faster behind the cold front in the experiments with the Anthes-Kuo scheme than the experiment with the Kain-Fritsch scheme, both the sensible and latent heat fluxes in the experiment with the Anthes-Kuo scheme behind the cold front are greater than those in the experiments with the Kain-Fritsch scheme.

These results indicate that interaction of the PBL scheme and the convective scheme plays a significant role in determining the surface fluxes, even more so than simply changing PBL schemes. The convective processes described by the convective parameterization schemes have an impact on the surface flux processes by changing the wind, temperature, and humidity at the

lowest model level where the surface fluxes are calculated. Therefore, when convection exists, the simulated surface fluxes are not only dependent on the choice of PBL schemes, but also on the convective parameterization schemes. This makes it difficult to directly validate the formulas used in the model for surface flux calculation under convective conditions. If, for example, the sensible heat flux at a location for a case is much different from the observations, it would be difficult to identify the cause as the surface flux/PBL scheme or the convective parameterization scheme.

5. DISCUSSION AND CONCLUSIONS

In this study, offshore mesoscale features of a land-falling cyclone simulated by a mesoscale model using different physics parameterization schemes are compared, along with their impact on the simulated coastal wind and precipitation. Great sensitivity of the simulated mesoscale features to various physics parameterization schemes is revealed by the comparison, indicating that the interaction of the PBL and the convective schemes is complicated.

Firstly, a great sensitivity is seen in the simulated frontal structure. The double structure of the cold front seen in the observations is more apparent in some experiments than others, and its strength varies with the convection schemes.

Secondly, the structure of the simulated LLJ varies greatly with different parameterization schemes, while the change in its intensity is relatively small. For example, the height of the LLJ can vary by as much as 680 m. Given that the average height of the LLJ is about 1.4 km, this variation can be significant. On the other hand, the variation of the maximum wind speed at the LLJ core (>30 m/s) varies no more than 3 m/s.

Thirdly, when the cold front and pre-frontal LLJ approach the bight region in southern California, the offshore fast low-level flow ahead of the cold front appears earlier and extends lower toward the surface with the Anthes-Kuo scheme than that with either the Kain-Fritsch or the Grell convective scheme. The onshore flow also indicates a sensitivity; in particular, the blocking of flow by the mountains lasts longer when the Anthes-Kuo convective scheme is used compared to when the other convective schemes are used.

Lastly, the onshore precipitation generated by the model shows significant sensitivity to the parameterization schemes. The experiments with the Anthes-Kuo convective scheme produce

significantly higher amounts of precipitation in the bight region of California than the experiments with either the Grell or the Kain-Fritsch schemes, indicating a strong sensitivity to the convective scheme. However, without the experiments using the Anthes-Kuo scheme, there is more sensitivity to the PBL scheme. While the precipitation amounts show a sensitivity, the location of the maximum precipitation in the bight region is not affected, because it is closely tied to ridge locations in that area of California.

All the results clearly suggest that the Anthes-Kuo scheme has deficiencies in producing realistic cloud patterns. Moreover, because the interaction of the scheme with all the PBL schemes tends to create a warmer surface air temperature, the surface fluxes in the Anthes-Kuo runs appear to be greater than those from the runs using the other convective schemes. All these deficiencies are revealed by examining different aspects of the model output from those that showed advantages of the scheme in the earlier studies (such as Wang and Seaman, 1997 and Bao et al., 2000). This is typical of model evaluation: the results are dependent on the definition of what constitutes a good model simulation/forecast.

It is also revealed in this study that with certain permutations of the combination of the convective parameterization schemes and PBL schemes, the model produces an along-cold front variation of wind speed/vorticity. Observations are needed to determine whether or not such a feature is realistic.

It should be pointed out that since only one case is investigated, the results from this study may not be enough to infer the general characteristics of the model's sensitivity to different physics parameterization schemes in the wind and precipitation predictions over the U.S. west coast during the winter season. A series of case studies like this one are required to provide statistically meaningful information in this regard.

Although model validation against observations is not meant to be the subject of this report, the issue deserves a few remarks because, in general, model validation includes the procedure of testing different parameterization schemes. Model validation requires first to define what the model is intended to do and what it is capable of doing. Unfortunately, it is impossible with a case study to summarize a list of phenomena that the model is capable of doing with a given resolution and the amount of information in the initial and boundary conditions. It is noticed in this study that the model reproduces the cyclone evolution, the double structure of the cold front, and the terrain induced precipitation maxima very well. Even for the timing of the

landfall of the LLJ and cold front, which are dominant factors in producing heavy rainfall and strong winds onshore, the model results provide good guidance. If these are the occurrences for which that the model is to be validated, our results indicate that the model should pass the test of validation. However, if the frontal structure, cloud physics, surface fluxes, PBL structure, and quantitative aspects of the terrain induced precipitation maxima were to be validated, one would immediately determine that for this particular case, the model shows uncertainties, and the sensitivity to the physics parameterization schemes is obvious. Therefore, observations of all these aspects should be available for validation. Even with availability of the observations, this case study, because of the model resolution and the analyses used for the initialization, would not guarantee a good picture of the performance of the model in the coastal wind and precipitation prediction. Only a long-term, persistent validation of model predictions with different parameterization schemes and various resolutions against systematic observations in the same region can provide such information.

6. REFERENCES

Anthes, R. A., 1977. A cumulus parameterization scheme for a one-dimensional cloud model. *Mon. Wea. Rev.* **105**: 270-286.

Bader, N. J., G. S. Forbes, J. R. Grant, R. B. E. Lilley, and A. J. Waters, 1995: *Images in Weather Forecasting: A Practical Guide for Interpreting Satellite and Radar Imagery.* Cambridge University Press, New York, NY, 499 pp.

Bao, J.-W., S.A. Michelson, J.M. Wilczak, F.M. Ralph, P.O.G Persson, and R.J. Zamora, 2000: *A case study of the impact of offshore P-3 observations on the prediction of coastal wind and precipitation.* NOAA Technical Memorandum OAR ETL-298, Environmental Technology Laboratory, Boulder, CO, 80303, 20 pp. (Available from the author or the National Technical Information Service, 5285 Port Royal Rd, Springfield, VA. 22161.)

Blackadar, A. K. ,1979. High resolution models of the planetary boundary layer. *Advances in Environmental Science and Engineering*, 1, No. 1. Pflafflin and Ziegler, eds., Gordon and Briech Sci. Publ., New York, 50-85.

Browning, K. A., and G. A. Monk, 1982. A simple model for synoptic analysis of cold fronts. *Quart. J. Roy. Meteorol. Soc.*, **108**, 435-452

Burk, S. D and, W. T. Thompson, 1989. A vertically nested regional numerical weather prediction model with second-order closure physics. *Mon. Wea. Rev.*, **117**, 2305–2324.

Dudhia, J.,1993. A nonhydrostatic version of the Penn State/NCAR mesoscale model: Validation tests and simulation of an Atlantic cyclone and cold front. *Mon. Wea. Rev.*, **121**, 1493-1513.

Grell , G. A., 1993. Prognostic evaluation of assumptions used by cumulus parameterizations. *Mon. Wea. Rev.*, **120**: 764-787.

Grell, G. A., J. Dudhia and D. R. Stauffer, 1994. A description of the fifth-generation Penn State/NCAR mesoscale model (MM5). NCAR Tech. Note, TN-398+STR, National Center for Atmospheric Research, Boulder, CO, 80307, 122 pp.

Hobbs, P V., P. O. G. Persson, 1982. The mesoscale and microscale structure and organization of clouds and precipitation in midlatitude cyclones. Part V: The substructure of narrow cold-frontal rainbands. *Jour. Atmos. Sci.*, **39**, 280–295.

Hong, S. -Y., and H. -L. Pan, 1996. Nonlocal boundary layer vertical diffusion in a medium-range forecast model. *Mon. Wea. Rev.*, **124**: 2322-2339.

Janjić, Z. I., 1994. The step-mountain eta coordinate model: Further developments of the convection, viscous sublayer, and turbulence closure schemes. *Mon. Wea. Rev.*, **122**, 927-945.

Kain, J. S., and J. M. Fritsch, 1993. Convective parameterization for mesoscale models: The Kain-Fritsch scheme. In: *The Representation of Cumulus Convection in Numerical Models, Meteor. Monogr.* No. 46, Amer. Meteor. Soc., 165-170.

Langland, R.H., R. Gelaro,, G.D. Rohaly. and M.A.Shapiro: 1999. Targeted observations in FASTEX: adjoint-based targeting procedures and data impact experiments in IOPs-17 and 18. *Quart. J. Roy. Meteorol. Soc.* **125**, 3241-3270.

Raymond, D.J., and K.A. Emanuel, 1993. The Kuo cumulus parameterization. *The Representation of Cumulus Convection in Numerical Models, Meteor. Monogr.* No. 46, Amer. Meteor. Soc., 145-147.

Somerville, R.C.J., 2000. Using single-column models to improve cloud-radiation parameterizations. *General Circulation Model Development*, D. Randall, ed., Academic Press, New York, New York, 641-657.

Wang, W. and N. L. Seaman, 1997. A comparison study of convective parameterization schemes in a mesoscale model. *Mon. Wea. Rev.* **125,** 252-278.

7. FIGURE CAPTIONS

Figure 1. Infrared satellite images at (a) 1200 UTC 2 Feb1998, (b) 0000 UTC 3 Feb, (c) 1200 UTC 3 Feb, and (d) 0000 UTC 4 Feb. Wind barbs are cloud track winds. Images can be found at:

http://willy.ssec.wisc.edu/~caljet/archive/winds/

Figure 2. Sea-level pressure and frontal analyses at (a) 1200 UTC 2 Feb (b) 0000 UTC 3 Feb, and (c) 1200 UTC (courtesy of P. J. Neiman)

Figure 3. The 36-km and 12-km grids used in all experiments.

Figure 4. Sea level pressure for (a) Experiment BLACKKF and (b) Experiment MRFAK at 1200 UTC 3 Feb. Contour interval is 2 mb.

Figure 5. 925 mb equivalent potential temperature at 1500 UTC 2 Feb for (a) MRFKF (b) MRFAK and (c) MRFGRELL. Contour interval is 2 K. Cf1 refers to the first cold front and cf2 refers to the second cold front. The heavy lines labeled AB and CD are the locations of the cross sections in Figure 6.

Figure 6. Cross section of equivalent potential temperature at 1500 UTC 2 Feb for (a) MRFKF and (b) MRFGRELL. Contour interval is 2 K. Cf1 and cf2 refer to the first and second cold fronts whose locations are indicated in Figure 5.

Figure 7. The height of the LLJ (km) at 1800 UTC 2 Feb as a function of the convective scheme.

Figure 8. The maximum wind speed (m/s) at 1800 UTC 2 Feb as a function of the convective scheme.

Figure 9. 925 mb wind speed (m/s) for experiment BTKF at (a) 1200 UTC 2 Feb and (b) 0600 UTC 3 Feb. Contour interval is 2 m/s

Figure 10. Same as Fig.#9 except for experiment MRFGRELL.

Figure 11. Accumulated precipitation (mm) for the 12 h period ending at 1200 UTC 3 Feb for experiment (a) MRFKF (b) MRFAK, and (c) MRFGRELL.

Figure 12. Model simulated dBz at 0600 UTC 3 Feb for experiment (a) MRFKF (b) MRFAK and (c) MRFGRELL overlaid with the average wind vectors from the surface to 3.0 km.

Figure 13. Time-height series of the wind (in knots) at a point off the coast of southern California to the west of the San Clemente and Santa Catalina islands from 1800 UTC 2 Feb to 1200 UTC 3

Feb for experiment (a) BLACKKF (b) BLACKAK, and (c) BLACKGRELL Winds are plotted at every model layer up to 4 km.

Figure 14. Same as Fig. #13 except for a point onshore near Santa Barbara in the bight region of southern California.

Figure 15. Sensible heat flux (W/m^2) for experiment (a) BLACKKF (b) BLACKAK, and (c) BLACKGRELL. Contour interval is 20 W/m^2.

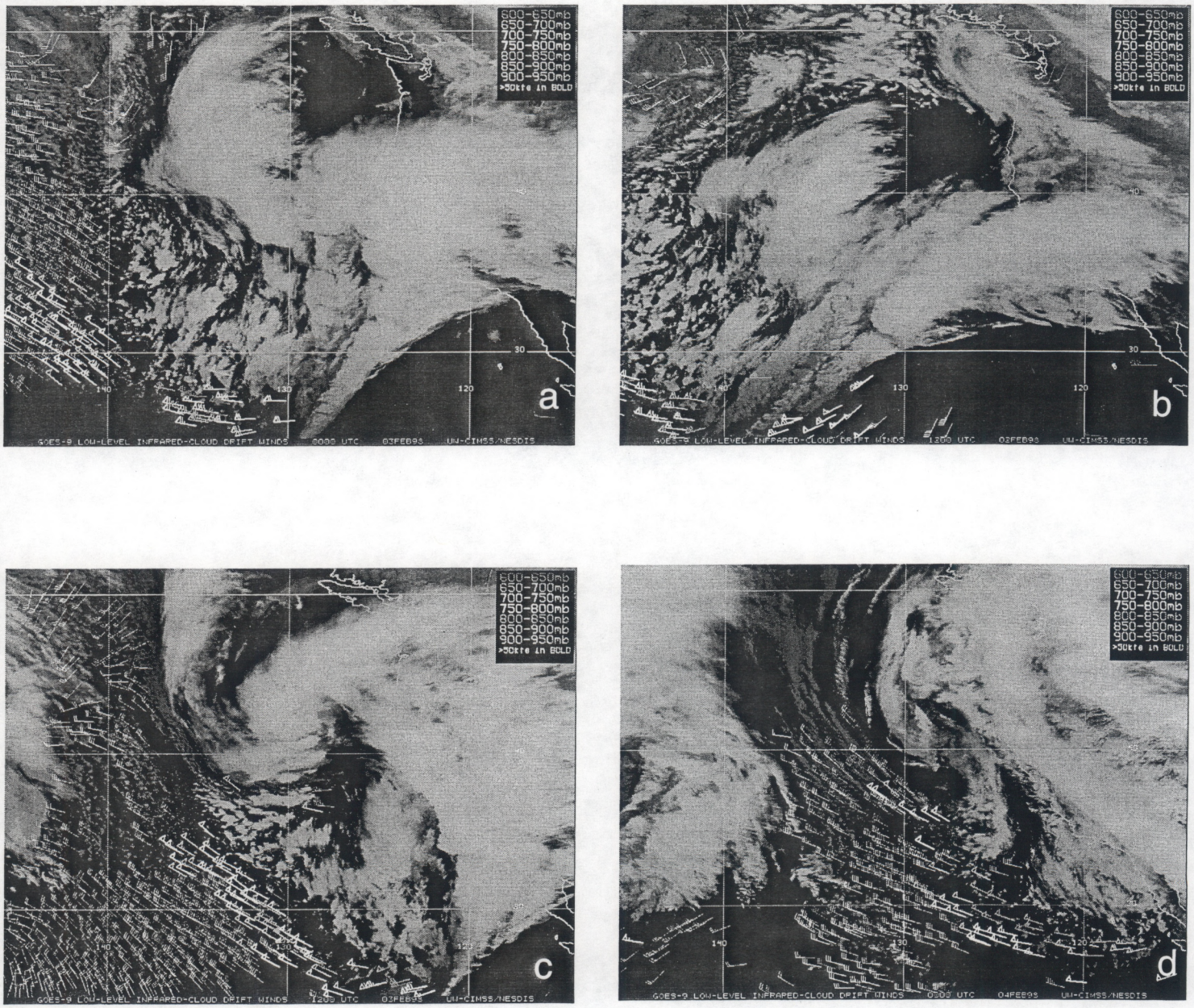

Figure 1. Infrared satellite images at (a) 1200 UTC 2 Feb, 1998 (b) 0000 UTC 3 Feb, (c) 1200 UTC 3 Feb, and (d) 0000 UTC 4 Feb. Wind barbs are cloud track winds. Images can be found at: http://willy.ssec.wisc.edu/~caljet/archive/winds/

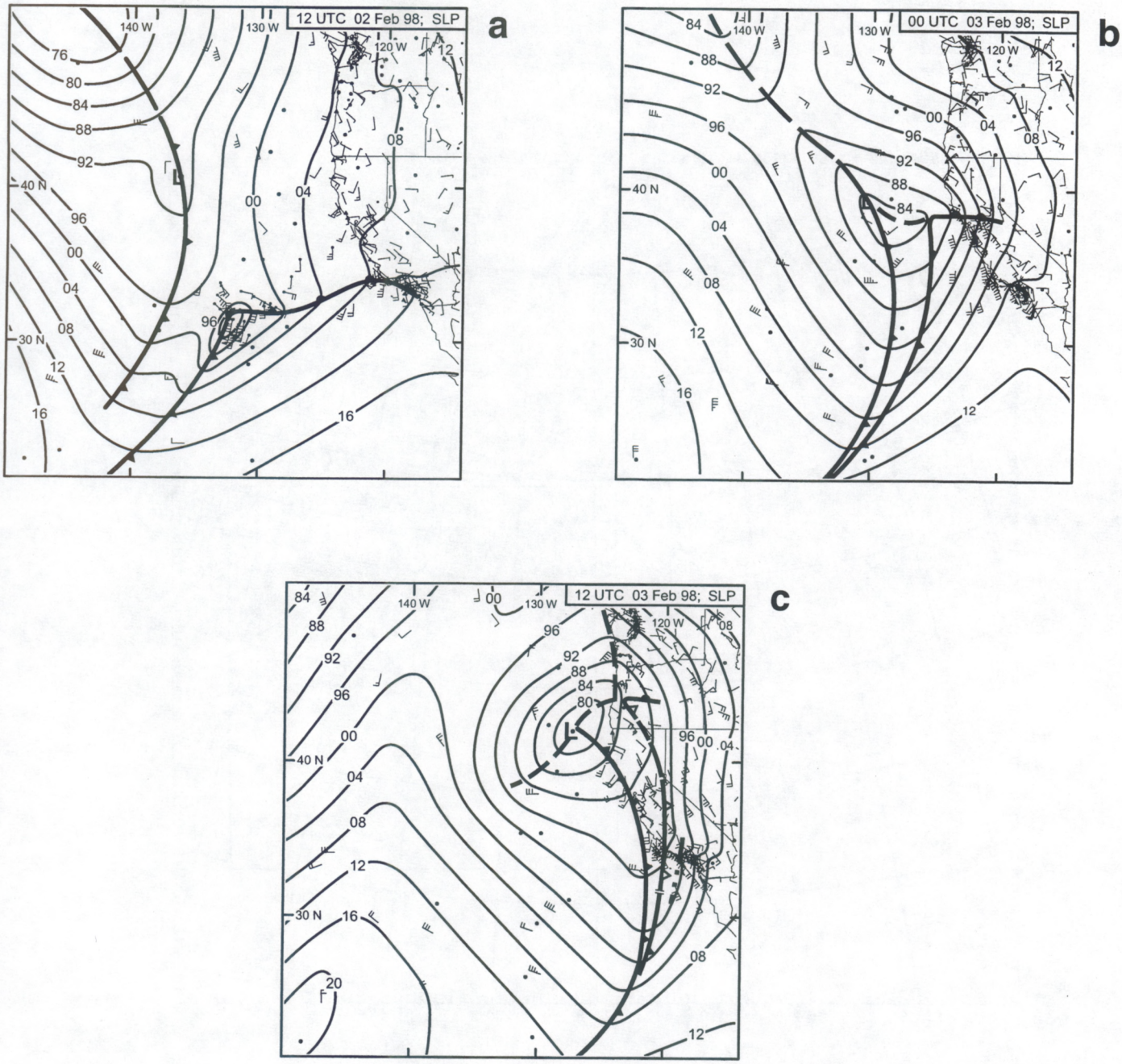

Figure 2. Sea level pressure and frontal analyses at (a) 1200 UTC 2 Feb (b) 0000 UTC 3 Feb, and (c) 1200 UTC (courtesy of P. J. Neiman)

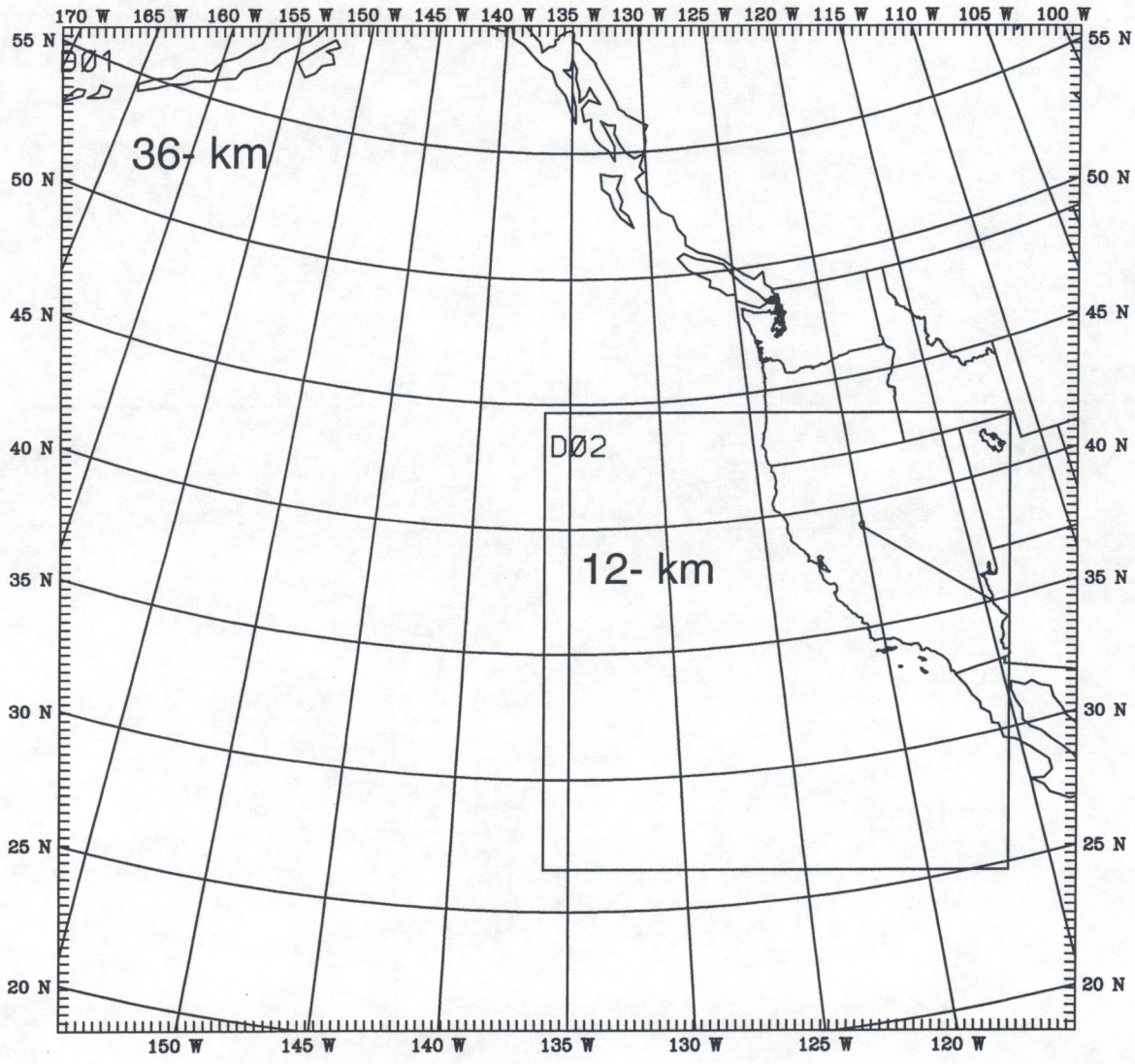

Figure 3. The 36-km and 12-km grids used in all experiments.

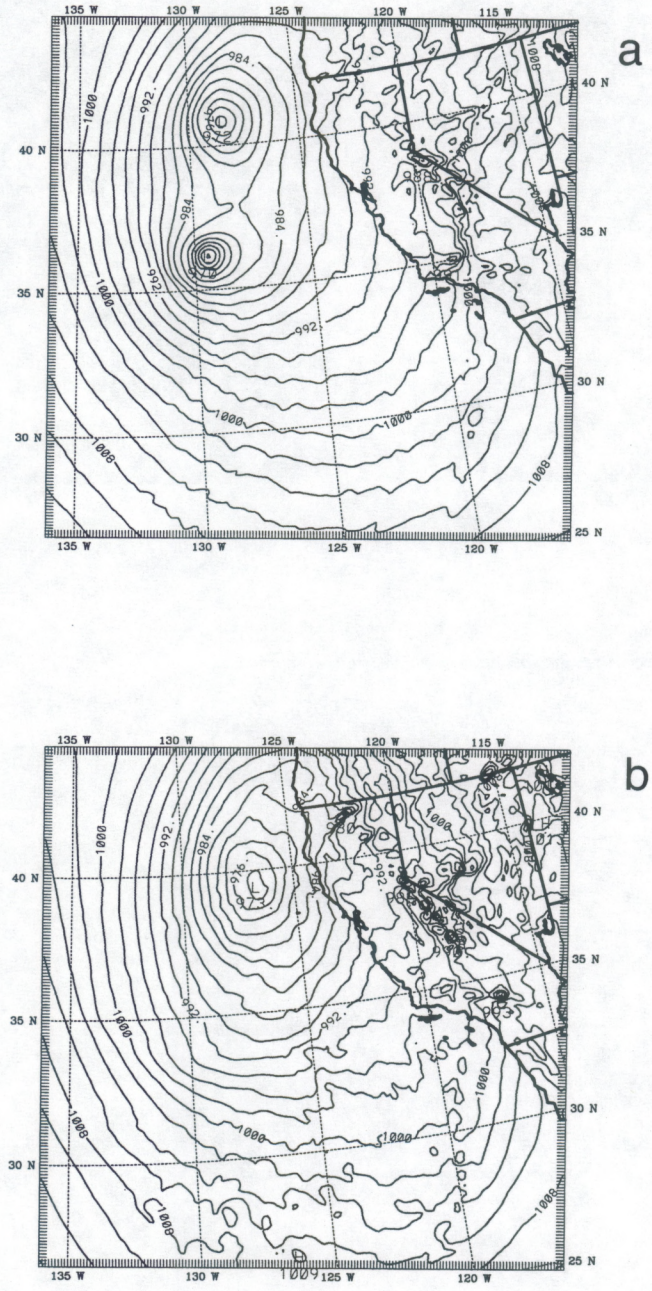

Figure 4. Sea-level pressure for (a) Experiment BLACKKF and (b) Experiment MRFAK at 1200 UTC 3 Feb. Contour interval is 2 mb.

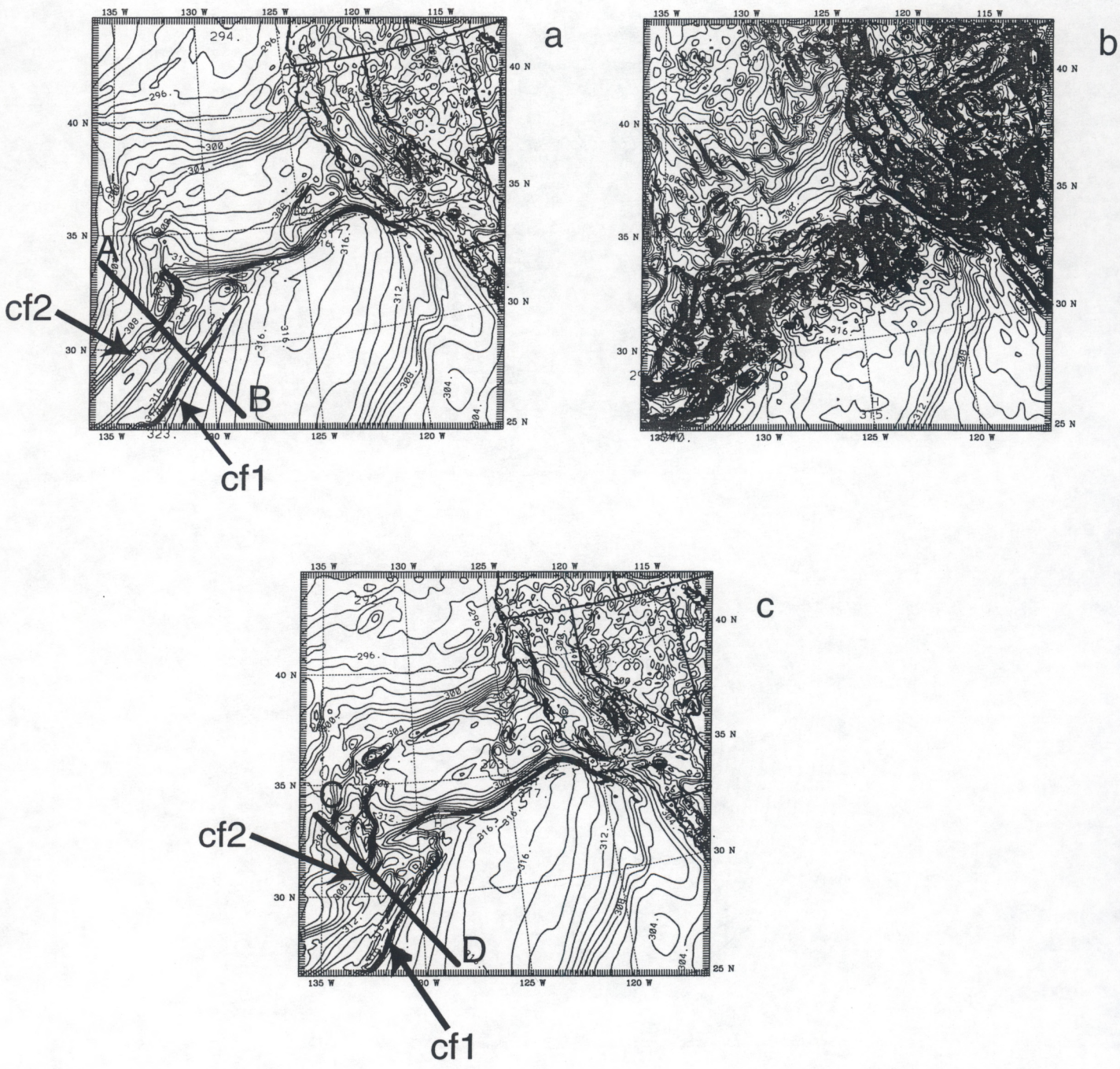

Figure 5. 925 mb equivalent potential temperature at 1500 UTC 2 Feb for (a) MRFKF (b) MRFAK and (c) MRFGRELL. Contour interval is 2 K. Cf1 refers to the first cold front and cf2 refers to the second cold front. The heavy lines labeled AB and CD are the locations of the cross sections in Figure 6.

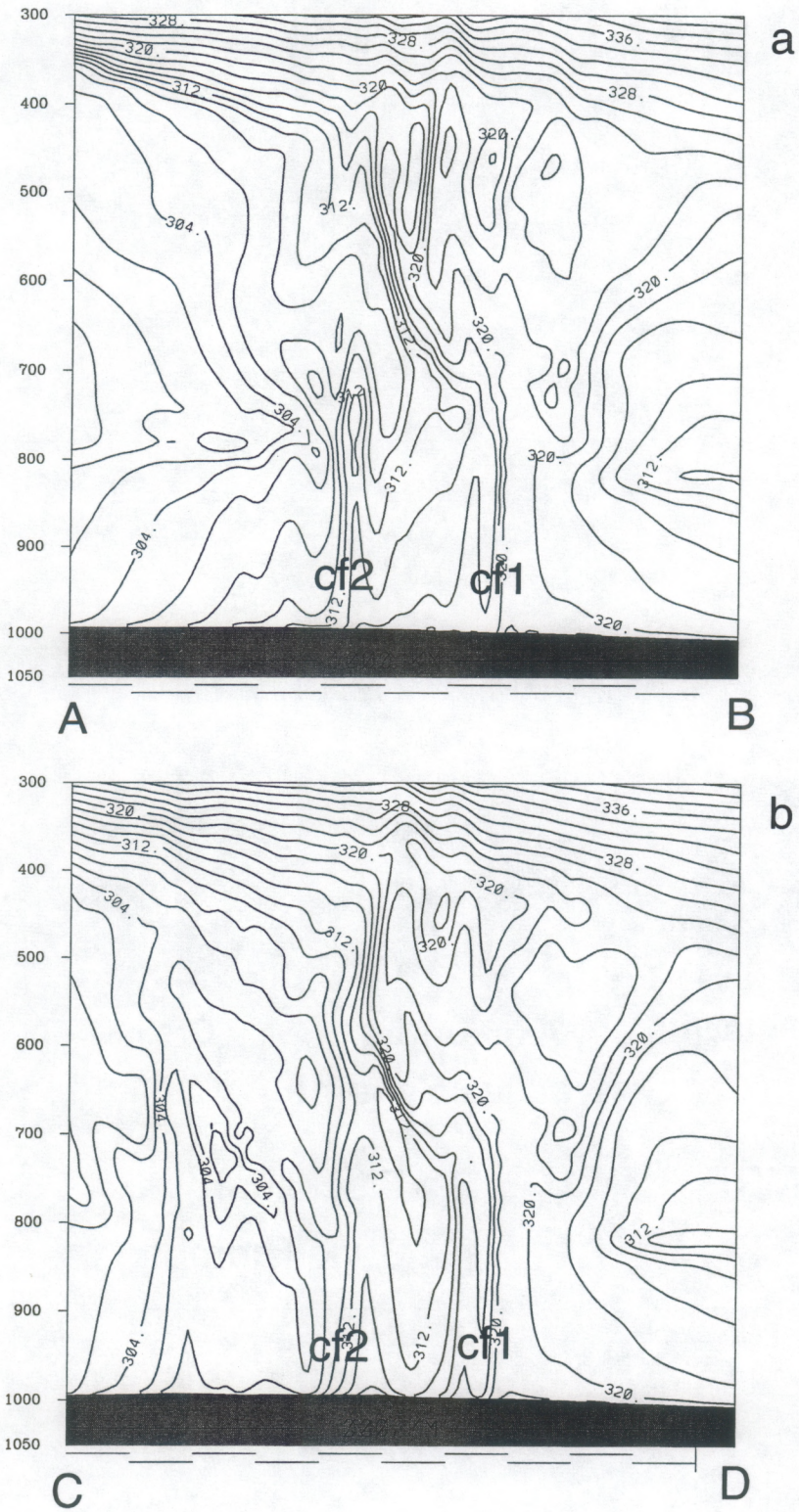

Figure 6. Cross section of equivalent potential temperature at 1500 UTC 2 Feb for (a) MRFKF and (b) MRFGRELL. Contour interval is 2 K. Cf1 and cf2 refer to the first and second cold fronts whose locations are indicated in Figure 5.

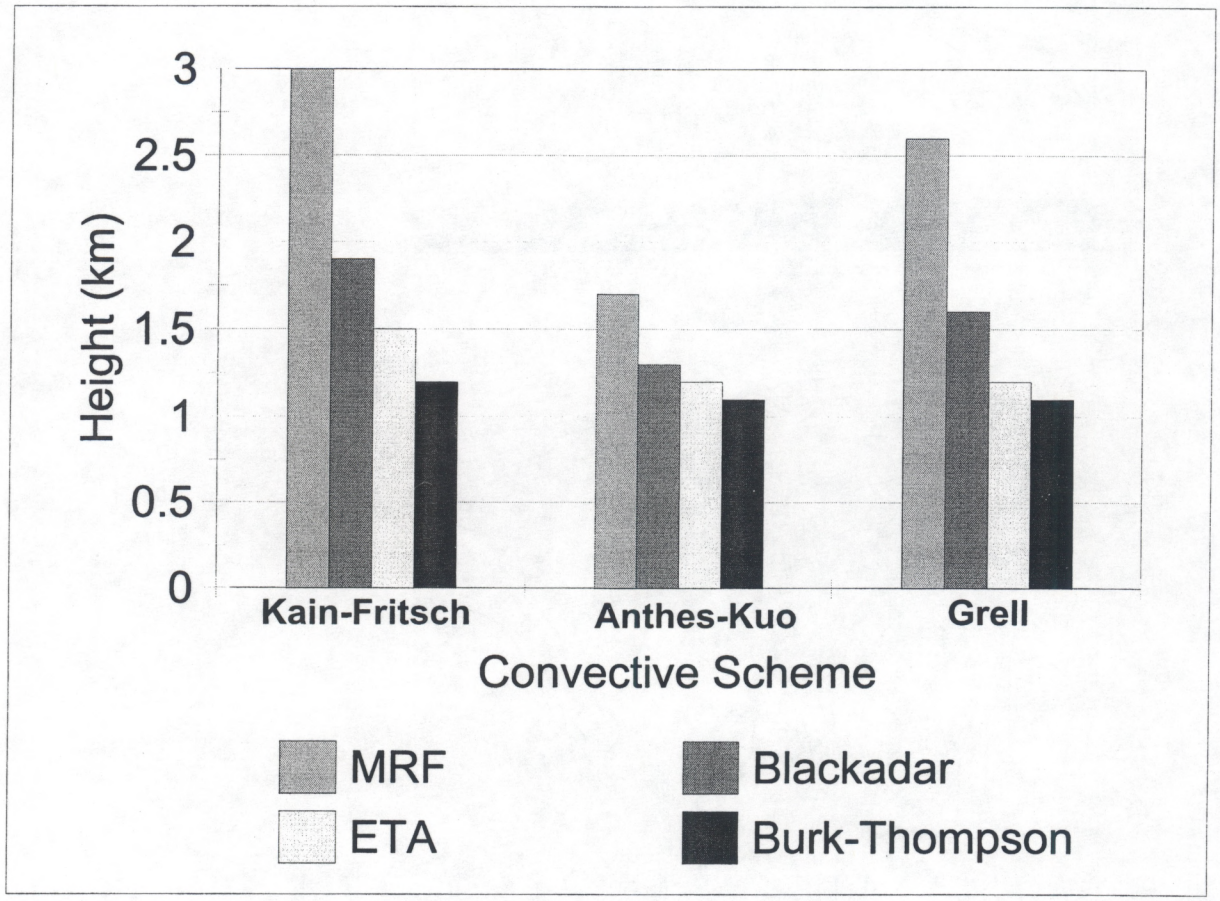

Figure 7. The height of the LLJ (km) at 1800 UTC 2 Feb as a function of the convective scheme.

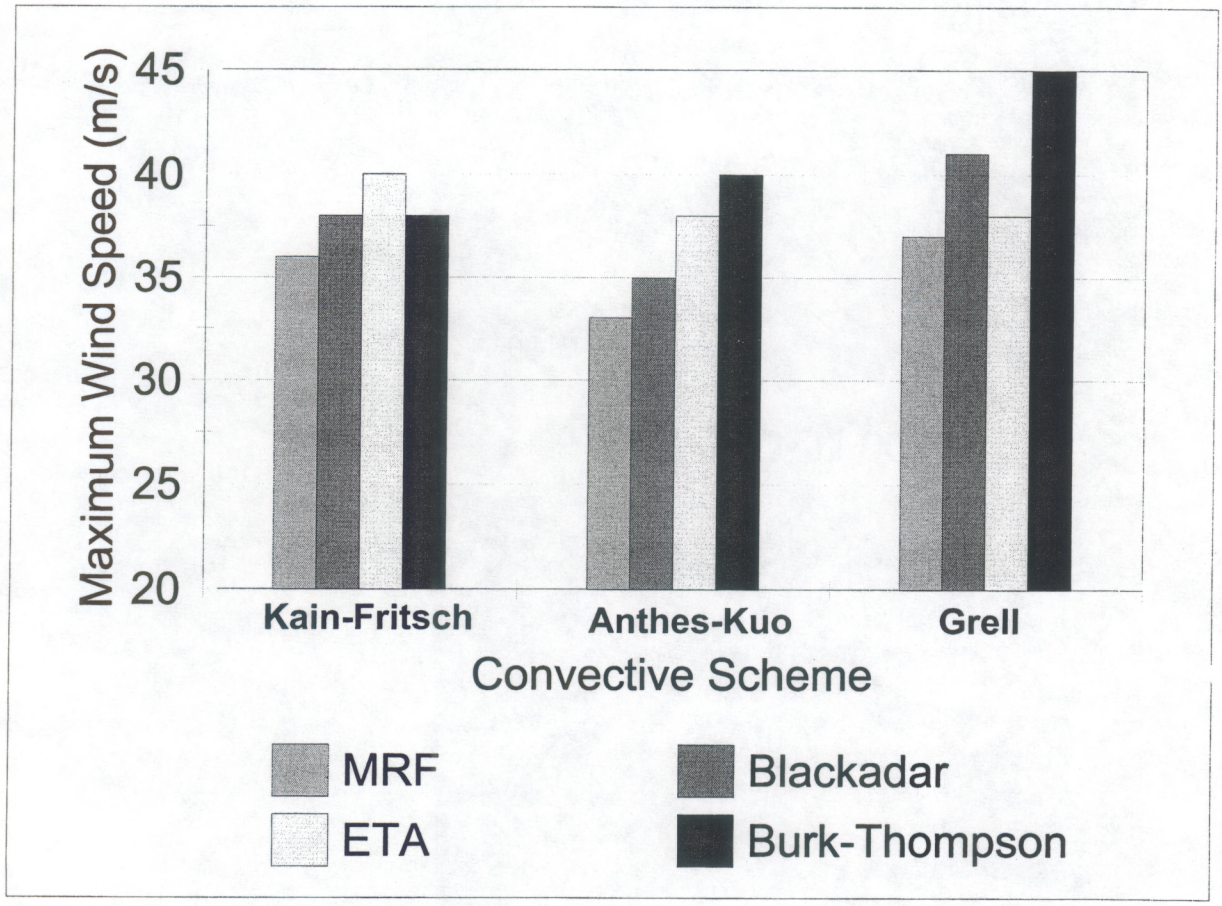

Figure 8. The maximum wind speed (m/s) at 1800 UTC 2 Feb as a function of the convective scheme.

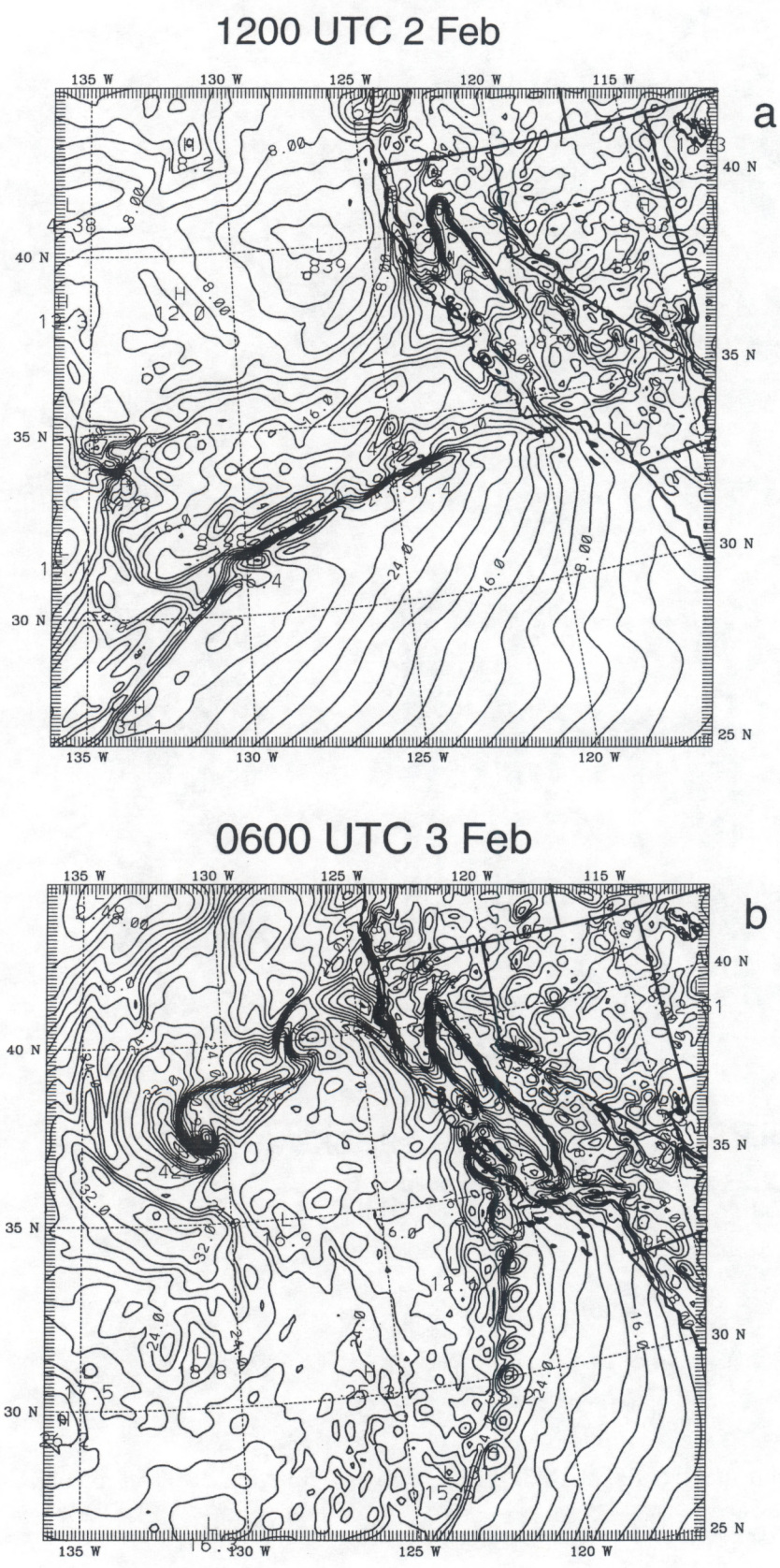

Figure 9. 925 mb wind speed (m/s) for experiment BTKF at (a) 1200 UTC 2 Feb and (b) 0600 UTC 3 Feb. Contour interval is 2 m/s

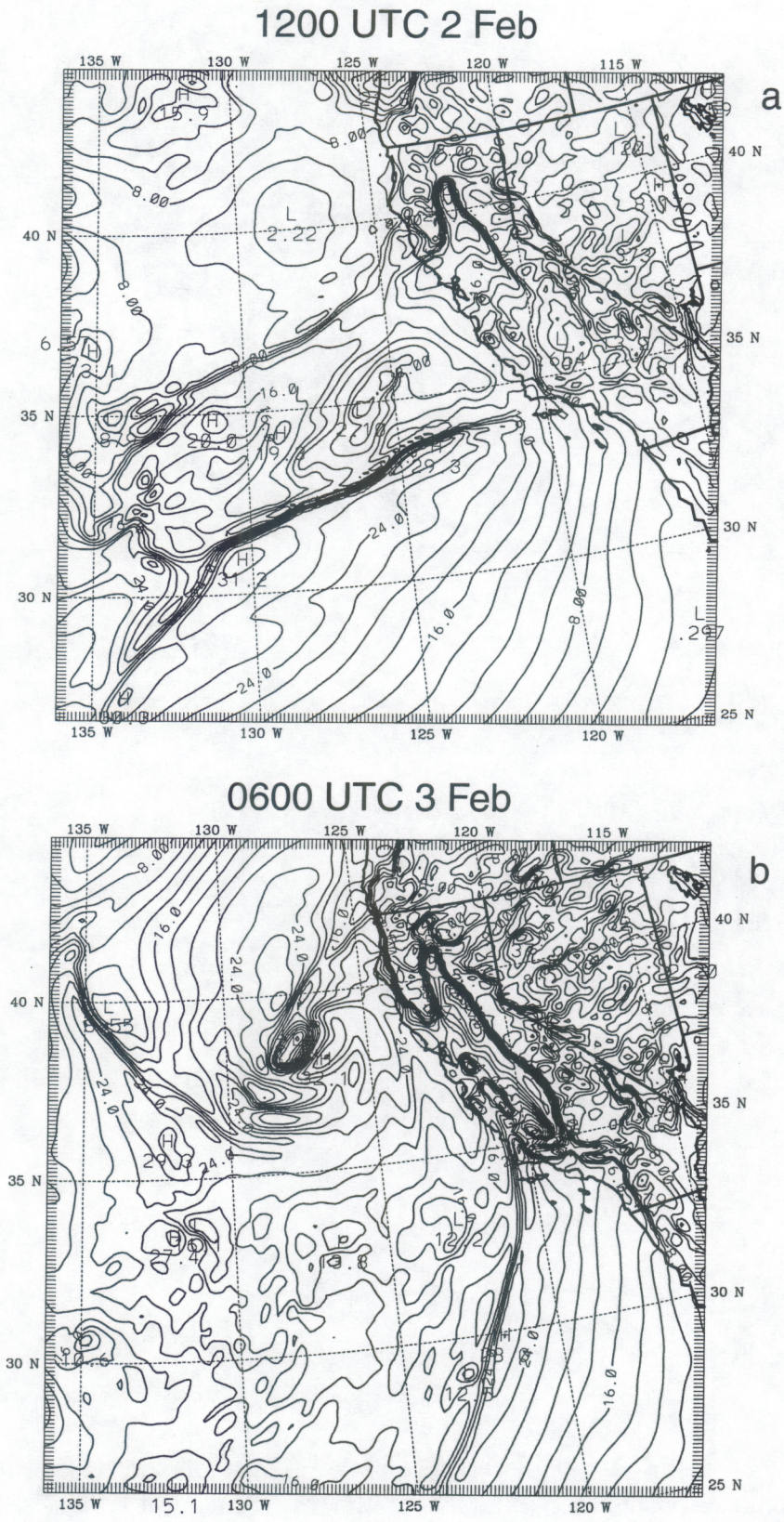

Figure 10. Same as Fig.#9 except for experiment MRFGRELL.

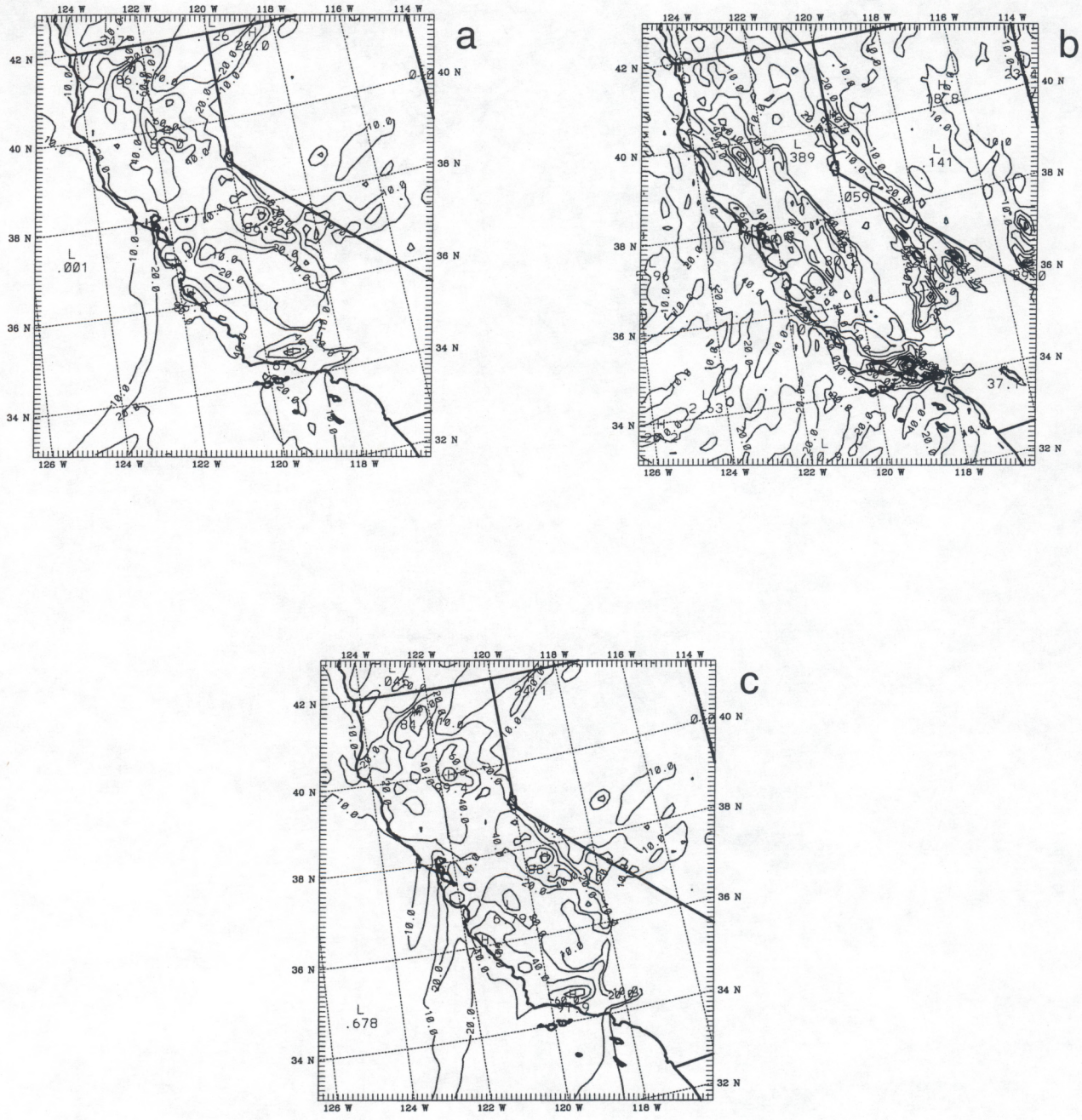

Figure 11. Accumulated precipitation (mm) for the 12 h period ending at 1200 UTC 3 Feb for experiment (a) MRFKF (b) MRFAK, and (c) MRFGRELL.

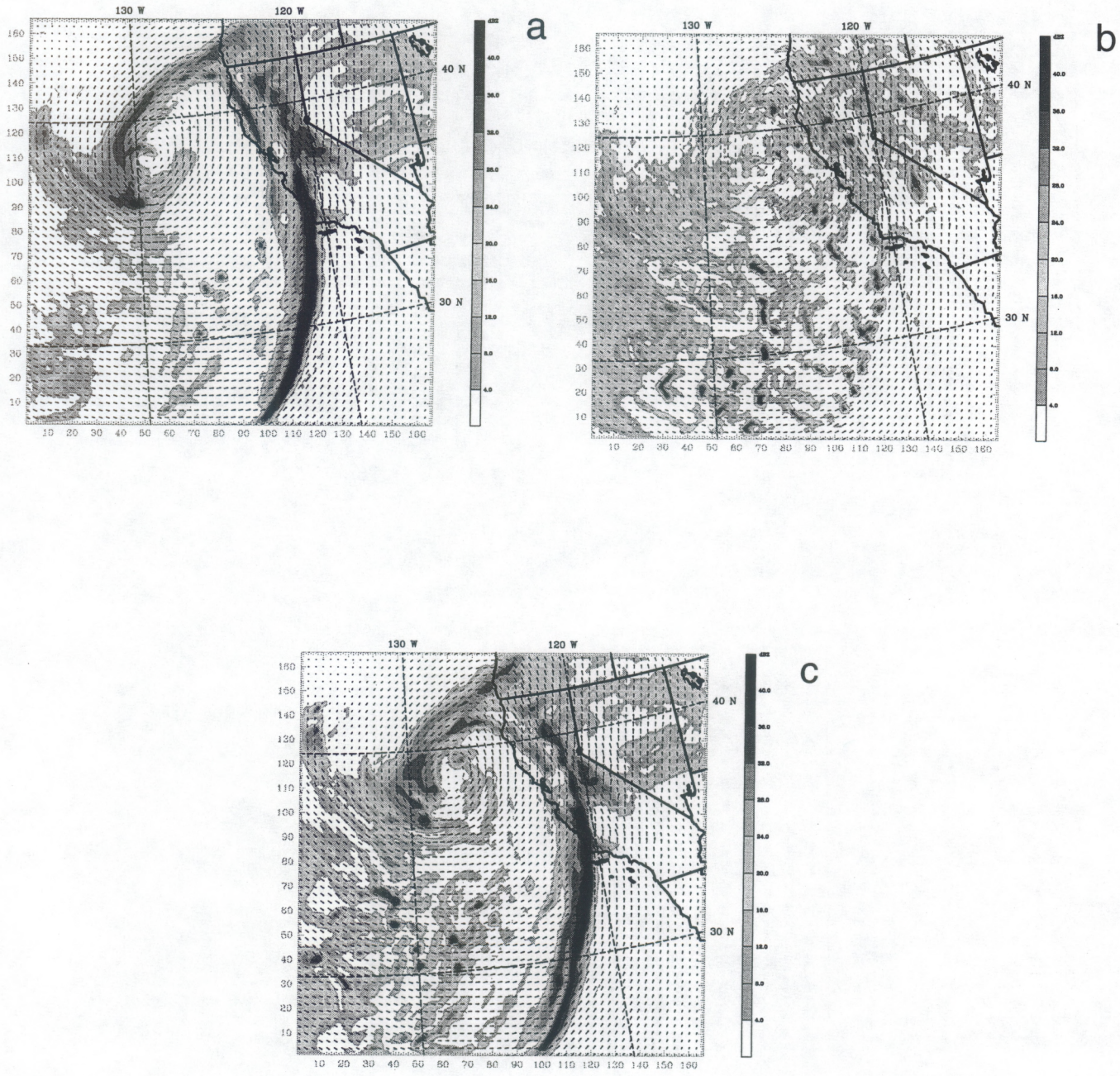

Figure 12. Model simulated dBz at 0600 UTC 3 Feb for experiment (a) MRFKF (b) MRFAK and (c) MRFGRELL overlaid with the average wind vectors from the surface to 3.0 km.

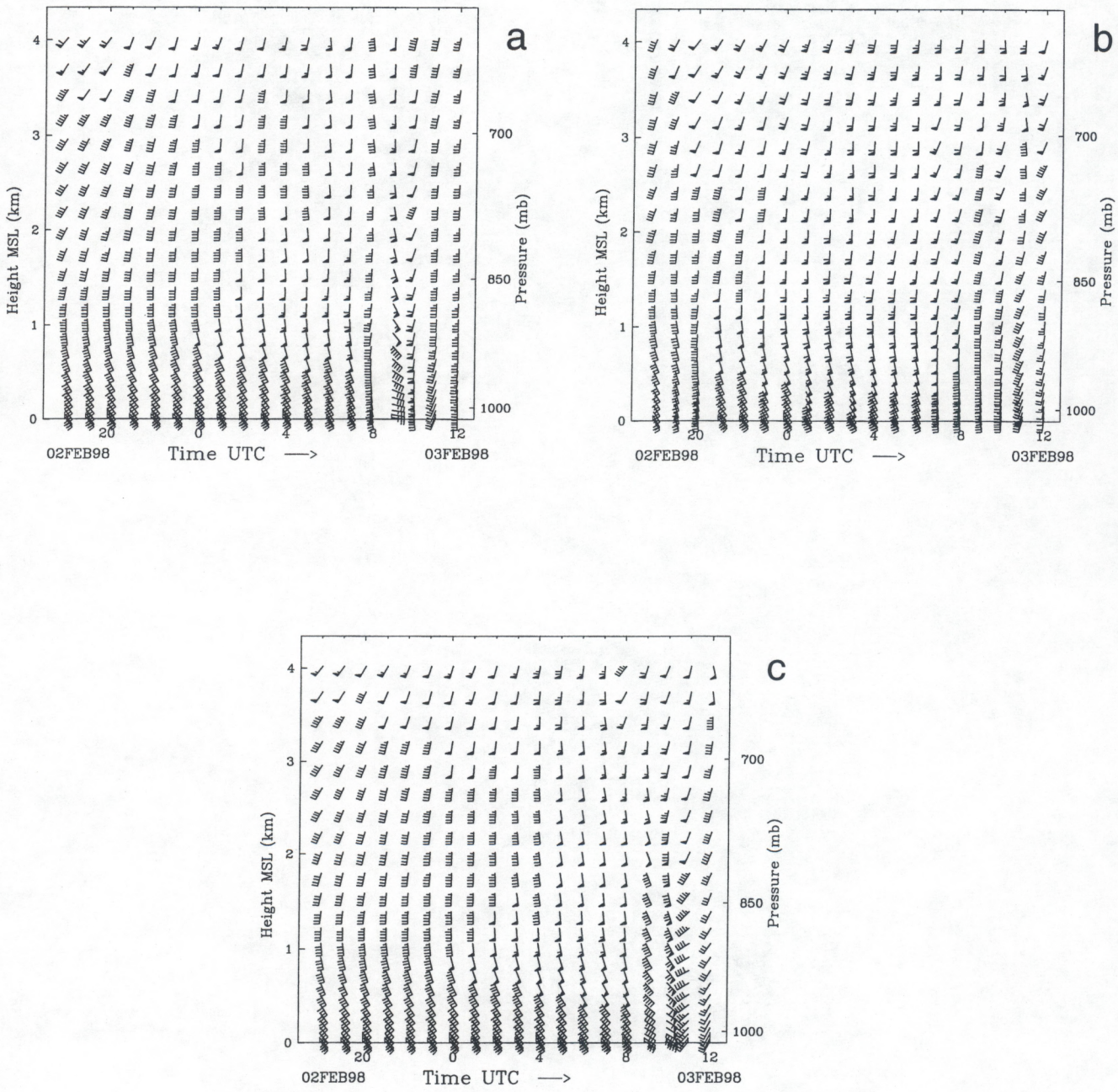

Figure 13. Time-height series of the wind (in knots) at a point off the coast of southern California to the west of the San Clemente and Santa Catalina islands from 1800 UTC 2 Feb to 1200 UTC 3 Feb for experiment (a) BLACKKF (b) BLACKAK, and (c) BLACKGRELL Winds are plotted at every model layer up to 4 km.

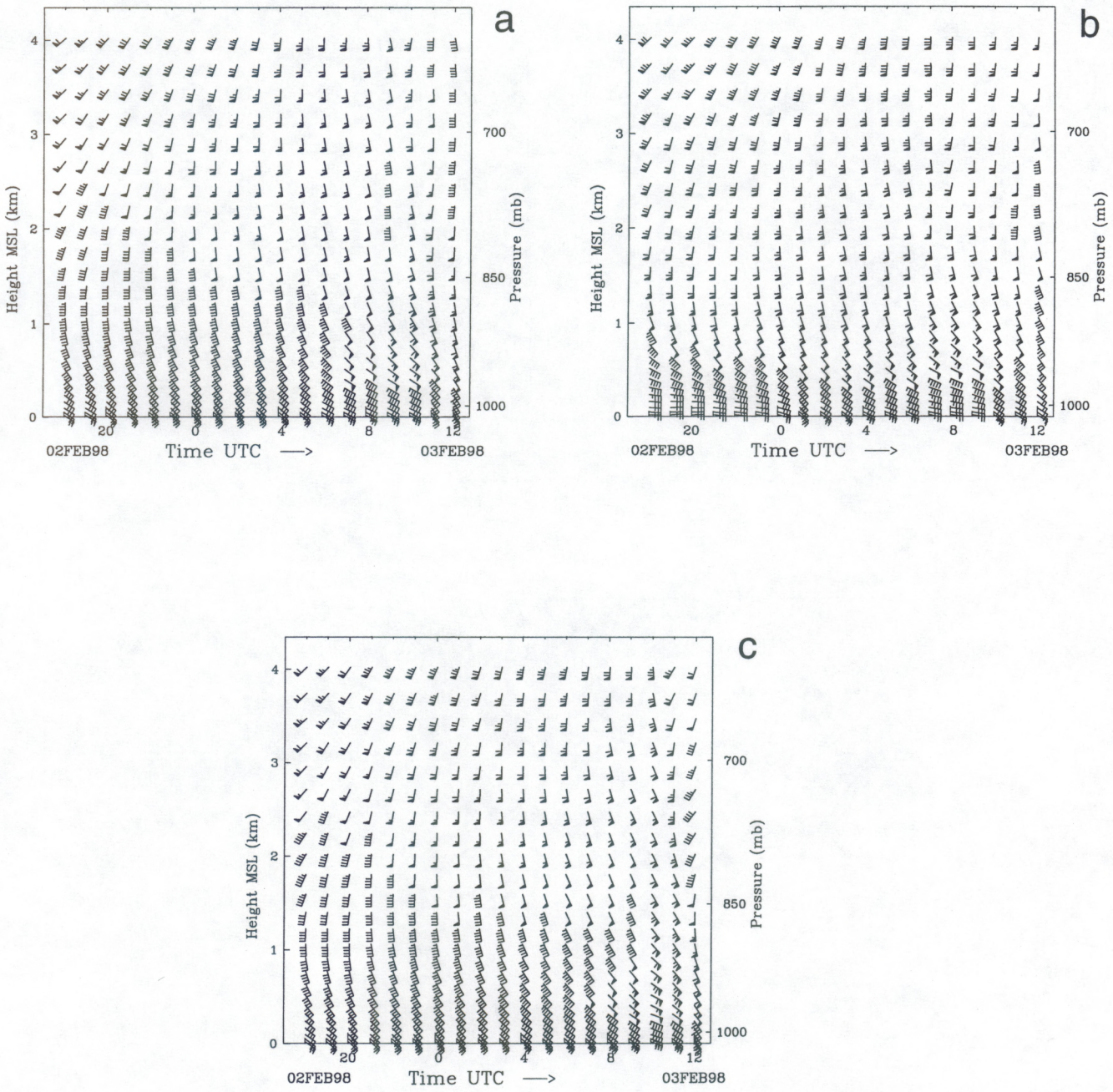

Figure 14. Same as Fig. #13 except for a point onshore near Santa Barbara in the bight region of southern California.

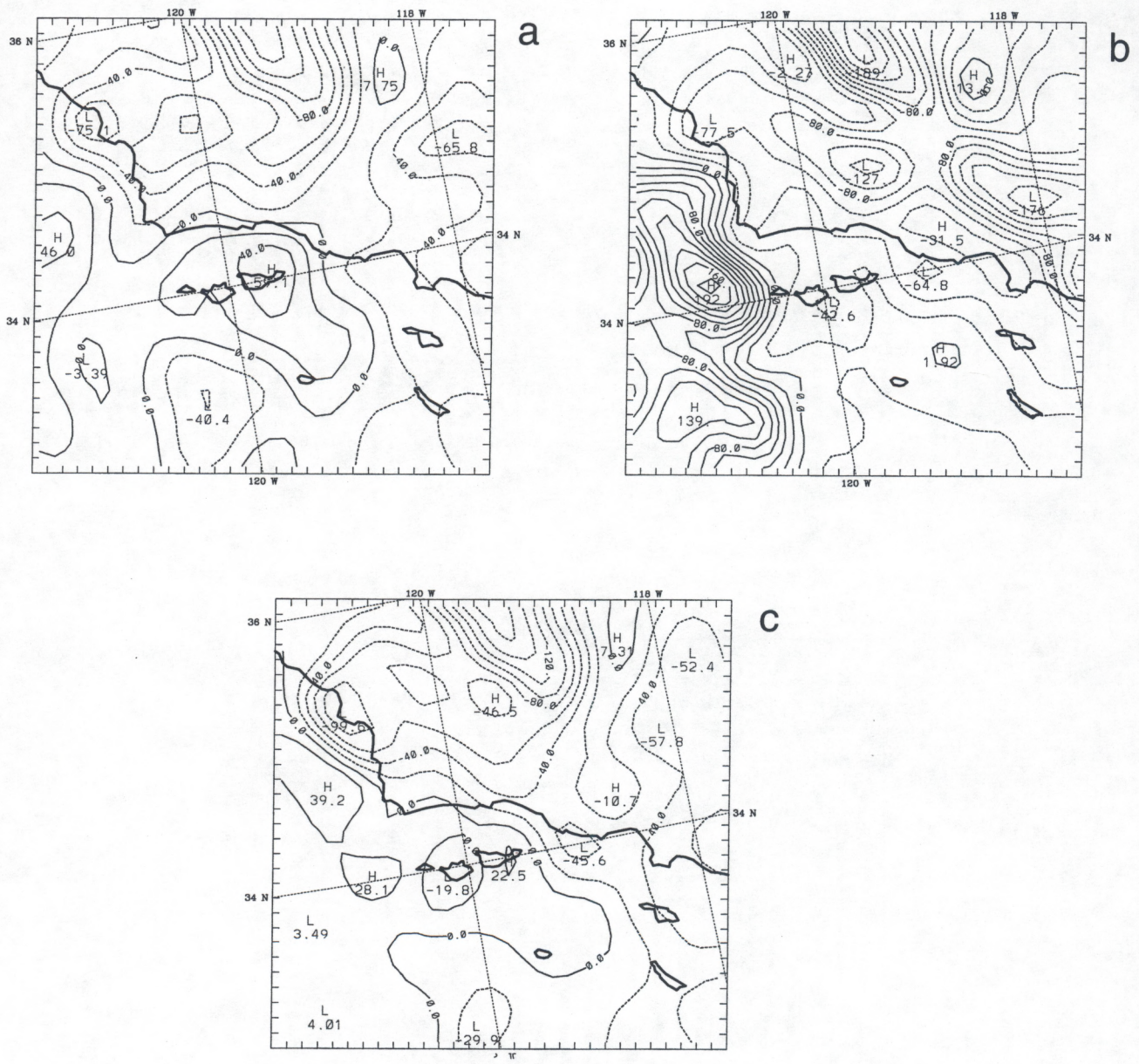

Figure 15. Sensible heat flux (W/m2) for experiment (a) BLACKKF (b) BLACKAK, and (c) BLACKGRELL. Contour interval is 20 W/m2.